Electronic Supplementary Information

Sulfonate group functionalized active carbon-based Cu catalyst for electrochemical ammonia synthesis under ambient conditions

Shengbo Zhang,[ab] Wenyi Li,[ab] Yanyan Liu,[ab] Jialu Wang,[ab] Guozhong Wang,[a] Yunxia Zhang,[a] Miaomiao Han,*[a] and Haimin Zhang*[a]

[a.] *Key Laboratory of Materials Physics, Centre for Environmental and Energy Nanomaterials, Anhui Key Laboratory of Nanomaterials and Nanotechnology, CAS Center for Excellence in Nanoscience, Institute of Solid State Physics, Chinese Academy of Sciences, Hefei 230031, China. E-mail:* mmhan@theory.issp.ac.cn, zhanghm@issp.ac.cn

[b.] *University of Science and Technology of China, Hefei 230026, China.*

Experimental Section

Synthesis of AC-S. All of the chemical regents were analytical grade (AR) and were used without further purification. AC-S was prepared by a direct hydrothermal method. The mixture of the 1.0 g of AC, 20 mL of sulfuric acid, and 2 mL of nitric acid was placed in 100 mL Teflon-lined stainless steel autoclave, which was heated in an oven at 110 °C K for 4 h. After the reaction, the autoclave was cooled down to room temperature. The resultant AC-S was collected and washed with deionized water and ethanol for several times in order to remove the residual reactants. Finally, the precipitate was dried in oven at 60 °C overnight.

Synthesis of Cu/AC-S. PVP and 30 mL ethanol were put in a three-neck flask under nitrogen atmosphere. The flask was vigorous stirred at room temperature. After this, a certain amount of $Cu(NO_3)_2.5H_2O$ was quickly added to the reaction mixture. Half an hour later, the $NaBH_4$ solution was cautiously added dropwise to the slurry, followed by centrifugation, washed with distilled water and ethanol until the pH < 7.0, and dried in a vacuum oven at 60 °C overnight.

Synthesis of Cu/AC. Cu/AC was prepared by using the same method except AC support was used instead.

Characterization. The crystalline structures of samples were identified by X-ray

diffraction analysis (XRD, Philips X'pert PRO) using Nifiltered monochromatic CuKa radiation ($\lambda K\alpha 1$ = 1.5418 Å) at 40 kV and 40 mA. Transmission electron microscope (TEM) images of samples were obtained using JEMARM 200F operating at an accelerating voltage of 200 kV. High-resolution transmission electron microscope (HRTEM), scanning TEM images (STEM) and elemental mapping images of samples were obtained on a JEOL-2010 transmission electron microscope. Furthermore, the spherical aberration corrected (Cs-corrected) high angle annular dark field scanning transmission electron microscopy (HAADF-STEM) and the energy-dispersive X-ray (EDX) mapping experiments were performed using FEI Titan G2 microscope equipped with a Super-X detector at 300 kV. X-ray photoelectron spectroscopy (XPS) analysis was performed on an ESCALAB 250 X-ray photoelectron spectrometer (Thermo, America) equipped with Al Kα1, 2 monochromatized radiations at 1486.6 eV Xray source. Nitrogen adsorption-desorption isotherms were measured using an automated gas sorption analyzer (Autosorb-iQ-Cx). The Cu $L_{3,2}$-edge X-ray absorptoion near-edge structure (XANES) spectra of samples were measured at BL12B-a beamline of NSRL in the total electron yield (TEY) mode by collecting the sample drain current under a vacuum better than 5×10^{-8} Pa. The beam from the bending magnet was monochromatized utilizing a varied linespacing plane grating and refocused by a toroidal mirror. The energy range is 100-1000 eV with an energy resolution of ca. 0.1 eV. The ^{15}N isotopic labeling experiments were conducted using $^{15}N_2$ as the feeding gas (99% enrichment of ^{15}N in $^{15}N_2$, Supplied by Hefei Ninte Gas Management Co., LTD). Prior to use for NRR measurements, $^{15}N_2$ feeding gas was purged through a 1.0 mM H_2SO_4 solution and distilled water to eliminate the potential NO_x and NH_3 contaminants.[2] The ^1H NMR (nuclear magnetic resonance) spectra were obtained using superconducting Fourier transform nuclear magnetic resonance spectrometer (Bruker Avance−400). $(^{15}NH_4)_2SO_4$ as reference samples was dissolved in 0.1 M Na_2SO_4 solution (D_2O/H_2O mixed solution, $V_{D2O}:V_{H2O}$ =1:4) for ^1H NMR measurements, and the electrolyte obtained from $^{15}N_2$-saturated 0.1 M Na_2SO_4 solution with the reaction time of 2 h and

concentration time of 12 h at 80 °C (D$_2$O/electrolyte mixed solution, V$_{D2O}$:V$_{electrolyte}$ =1:4) for ^{1}H NMR measurements.

Electrochemical measurements. All electrochemical measurements were performed on a CHI 660E electrochemical workstation (CH Instrumental Corporation, Shanghai, China) using a two-compartment cell, which was separated by Nafion 117 proton exchange membrane. Different catalyst inks were prepared by dispersing 2.5 mg sample into 100 µL of ethanol and 5.0 µL of Nafion (5.0 wt.%) under ultrasonic, and were then dropped on carbon cloth with 1×1 cm^2 used as the working electrode. A Ag/AgCl electrode was used as the reference electrode and a Pt wire was used as the counter electrode. The polarization curves were measured with a scan rate of 5.0 mV s^{-1} at room temperature and all polarization curves were obtained at the steady-state ones after several cycles. For N$_2$ reduction reaction (NRR) experiments, the potentiostatic test was conducted for 2 h in N$_2$-saturated 0.1 M Na$_2$SO$_4$ solution (30 mL, pH=6.3) by continuously supplying N$_2$ into the electrolyte under ambient conditions. Prior to NRR measurements, N$_2$ feeding gas was first purged through a 1.0 mM H$_2$SO$_4$ solution and distilled water to eliminate the potential NO$_x$ and NH$_3$ contaminants. In this work, all measured potentials (*vs.* Ag/AgCl) were transformed into the potentials *vs.* reversible hydrogen electrode (RHE) based on the following equation:

$$E_{RHE} = E_{Ag/AgCl} + 0.059pH + E°_{Ag/AgCl}$$

Determination of ammonia. Concentration of the produced ammonia was spectrophotometrically detected by the indophenol blue method. In detail，2 mL of sample was taken, and then diluted with 8 mL of deionized water. Subsequently, 100 µL of oxidizing solution (sodium hypochlorite (ρCl=4~4.9) and 0.75 M sodium hydroxide), 500 µL of colouring solution (0.4 M sodium salicylate and 0.32 M sodium hydroxide) and 100 µL of catalyst solution (0.1g Na$_2$[Fe(CN)$_5$NO]·2H$_2$O diluted to 10 mL with deionized water) were added respectively to the measured sample solution. After the placement of 1 h in room temperature, the absorbance measurements were performed at wavelength of 697.5 nm. The obtained calibration

curve (Fig. S7) was used to calculate the ammonia concentration.

Determination of hydrazine. The hydrazine present in the electrolyte was estimated by the method of Watt and Chrisp. A mixture of para-(dimethylamino) benzaldehyde (5.99 g), HCI (concentrated, 30 mL) and ethanol (300 mL) was used as a color reagent. In detail, 2 mL of sample was taken, and then diluted with 8 mL 0.1 M HCl solution. Subsequently, 5 mL of the prepared color reagent was added to the above sample solution. Subsequently, the absorbance measurements were performed after the placement of 20 min at wavelength of 455 nm. The obtained calibration curve (Fig. S8) was used to calculate the $N_2H_4·H_2O$ concentration.

Calculations of NH$_3$ yield rate and Faradaic efficiency.

The equation of NH$_3$ yield rate:

$$R(NH_3)(\mu g \ h^{-1} \ mg^{-1}) = \frac{C(NH_4^+ - N)(\mu g \ mL^{-1}) \times V(mL) \times 17}{t(h) \times m(mg) \times 14}$$

where R (NH$_3$) is the ammonia yield rate; C (NH$_4^+$-N) is the measured mass concentration of NH$_4^+$-N; V is the electrolyte solution volume; t is the reaction time; 14 is the molar mass of NH$_4^+$-N atom; 17 is the molar mass of NH$_3$ molecules; and m was the loading mass of catalysts.

The equation of Faradaic efficiency:

$$FE(NH_3)(\%) = \frac{3 \times n(NH_3)(mol) \times F}{Q} \times 100\%$$

where F is the Faradaic constant (96485.34); Q is the total charge during the NRR.

Supplementary Tables and Figures

Table S1. The comparable results of our work and other recently reported NRR electrocatalysts.

References	Catalyst	System /Conditions	NH$_3$ Production Rate	Faradaic Efficiency (%)	Detection method
		Noble metal electrocatalyst			
1	Pd nanoparticles	0.1 M PBS	4.2 µg mg^{-1} h^{-1} (0.1 V *vs.* RHE)	8.2	Indophenol method
2	Au nanorods	0.1 M KOH	1.648 µg h^{-1} cm^{-2} (-0.2 V *vs.* RHE)	4.02	Nessler's reagent
3	Au/TiO$_2$	0.1 M HCl	21.4 µg mg^{-1} h^{-1} (-0.2 V *vs.* RHE)	8.11	Indophenol method
4	α-Au/CeO$_x$-RGO	0.1 M HCl	8.3 µg mg^{-1} h^{-1} (-0.2 V *vs.* RHE)	10.1	Indophenol method
5	Pd$_{0.2}$/Cu$_{0.8}$ nanoclusters	0.1 M KOH	1.66 µg mg^{-1} h^{-1} (-0.2 V *vs.* RHE)	4.52	Indophenol method
6	Ag nanosheets	0.1 M HCl	2.8µg h^{-1} cm^{-2} (-0.6 V *vs.* RHE)	4.8	Indophenol method
7	Rh nanosheet	0.1 M KOH	23.88 µg cm^{-2} h^{-1} (-0.2 V *vs.* RHE)	0.217	Indophenol method
8	Au nanocages	0.5 M LiClO$_4$	3.74 µg cm^{-2} h^{-1} (-0.4 V *vs.* RHE)	35.9	Nessler's reagent
9	Ru/MoS$_2$	0.01M HCl	1.14 × 10^{-10} mol cm^{-2} s^{-1} (-0.15 V *vs.* RHE)	17.6	Indophenol method
10	Ag-Au@ZIF	LiCF$_3$SO$_3$ 1% EtOH in THF	10 pmol cm^{-2} s^{-1} (-2.9 V *vs.* Ag/AgCl)	18±4	Indophenol method
11	pAu/NF	0.1 M Na$_2$SO$_4$	9.42 µg cm^{-2} h^{-1} (-0.2 V *vs.* RHE)	13.36	Indophenol method
12	AuSAs-NDPCs	0.1M HCl	2.32 µg cm^{-2} h^{-1} (-0.3 V *vs.* RHE)	12.3	Indophenol method
13	BiNCs	0.5 M K$_2$SO$_4$	200 mmol g^{-1} h^{-1}	66	Nessler's reagent
		Metal free catalyst			
14	N-doped porous carbon	0.05 M H$_2$SO$_4$	23.8 µg mg^{-1} h^{-1} (-0.9 V *vs.* RHE)	1.42	Indophenol method

15	Polymeric carbon nitride	0.1 M HCl	8.09 µg mg^{-1} h^{-1} (-0.2 V $vs.$ RHE)	11.59	Indophenol method
16	NPC-500	0.005 M H$_2$SO$_4$	22.3 µg mg^{-1} h^{-1} (-0.4 V $vs.$ RHE)	9.58	Indophenol method
17	B$_4$C nanosheet	0.1 M HCl	26.57 µg mg^{-1} h^{-1} (-0.75 V $vs.$ RHE)	15.95	Indophenol method
Transition metal catalyst					
18	Fe$_2$O$_3$-CNTs	diluted KHCO$_3$ aqueous solution	0.22 µg mg^{-1} h^{-1} （-1.0V $vs.$ Ag/AgCl）	0.15	Indophenol method
19	MoS$_2$/CC	0.1 M Na$_2$SO$_4$	4.94 µg mg^{-1} h^{-1} (-0.5 V $vs.$ RHE)	1.17	Indophenol method
20	Mo nanofilm	0.01 M H$_2$SO$_4$	1.89 µg mg^{-1} h^{-1} (-0.14 V $vs.$ RHE)	0.72	Indophenol method
21	MoS$_2$ nanosheet	0.1 M Li$_2$SO$_4$	43.4 µg h^{-1} mg$_{MoS2}^{-1}$ (-0.2 V $vs.$ RHE)	9.81	Indophenol method
22	CoS$_2$/NS-G	0.05 M H$_2$SO$_4$	25.0 µg mg^{-1} h^{-1} (-0.2 V $vs.$ RHE)	25.9 (-0.05 V $vs.$ RHE)	Indophenol method
23	CuO/RGO	0.1 M Na$_2$SO$_4$	1.8 × 10^{-10} mol cm^{-2} s^{-1} (-0.75 V $vs.$ RHE)	3.9	Indophenol method
24	FeMoS	0.1 M HCl	8.45 µg mg^{-1} h^{-1} (-0.5 V $vs.$ RHE)	2.96	Indophenol method
25	W$_2$N$_3$	0.1 M HCl	11.66 ± 0.98 µg mg^{-1} h^{-1} (-0.2 V $vs.$ RHE)	11.67 ± 0.93	Indophenol method
Single-atom catalyst					
26	Au SAs/C$_3$N$_4$	0.005 M H$_2$SO$_4$	1305 µg h^{-1} mg$_{Au}^{-1}$ (-0.2 V $vs.$ RHE)	11.1	Indophenol method
27	Ru SAs/N-C	0.05 M H$_2$SO$_4$	120.9 µg h^{-1} mg$_{cat}^{-1}$ (-0.2 V vs. RHE)	29.6	Indophenol method
28	Ru@ZrO$_2$/NC	0.1 M HCl	3665 µg h^{-1} mg$_{Ru}^{-1}$ (-0.21 V vs. RHE)	21	Indophenol method
29	SA-Mo/NPC	0.1 M KOH	34.0 ± 3.6 µg h^{-1} mg$_{cat}^{-1}$ (-0.3 V vs. RHE)	14.6 ± 1.6	Indophenol method

30	Fe$_{SA}$-N-C	0.1 M KOH	7.48 µg h^{-1} mg$_{cat}^{-1}$ (0 V vs. RHE)	56.55	Indophenol method
31	ISAS-Fe-N-C	0.1 M PBS	62.9 ± 2.7 µg h^{-1} mg$_{cat}^{-1}$ (-0.4 V vs. RHE)	18.6 ± 0.8	Indophenol method
32	Mo^0/GDY	0.1 M Na$_2$SO$_4$	145.4 µg mg^{-1} h^{-1} (-1.2 V $vs.$ SCE)	21	Indophenol method
This work	Cu/AC-S	0.1 M Na$_2$SO$_4$	or 9.7 µg h^{-1} mg^{-1} (-0.3 V $vs.$ RHE)	15.9	Indophenol method
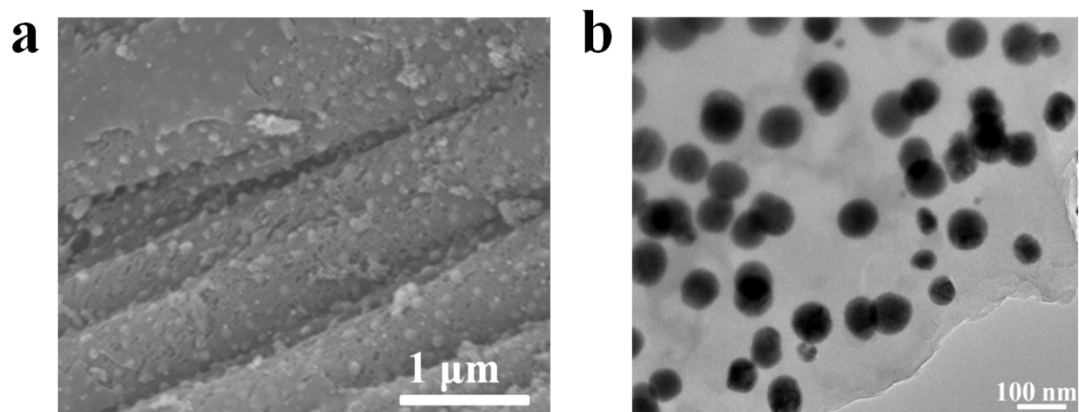
Fig. S1 (a) SEM and (b) TEM images of Cu/AC.
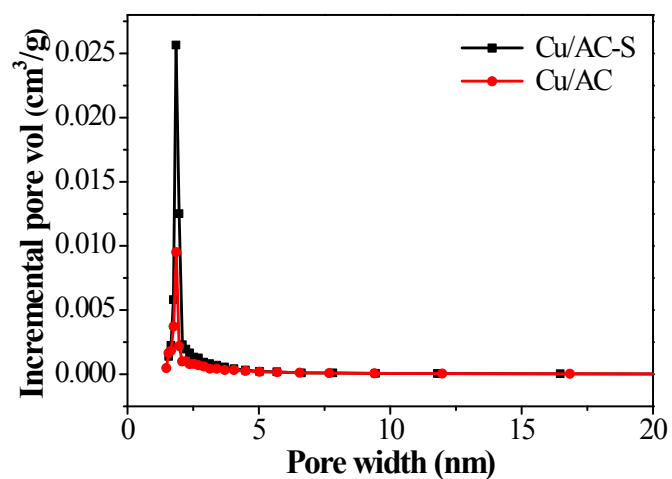
Fig. S2 The pore size distribution curve of Cu/AC and Cu/AC-S.
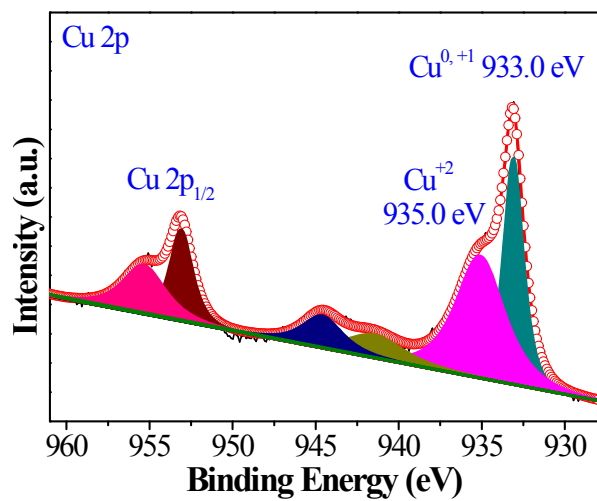
Fig. S3 Cu 2p XPS spectrum of Cu/AC.
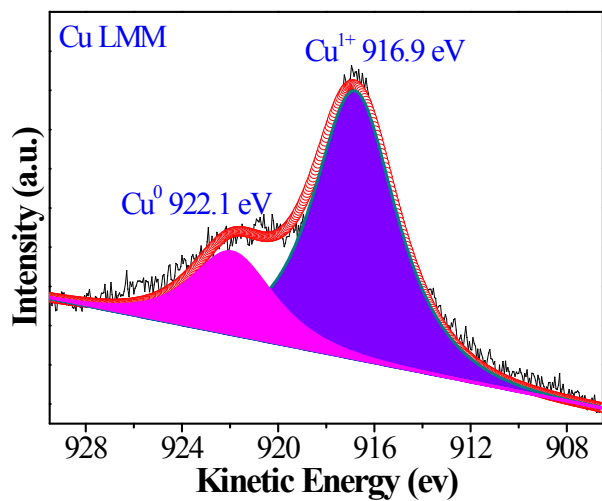
Fig. S4 Cu LMM XPS spectrum of Cu/AC-S.
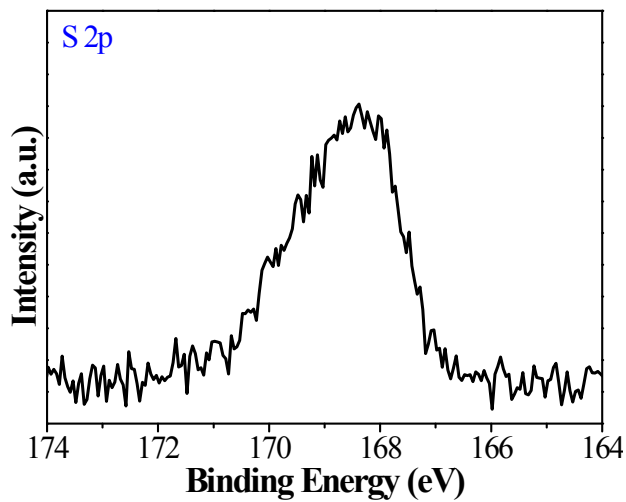
Fig. S5 S 2p XPS spectrum of Cu/AC-S.
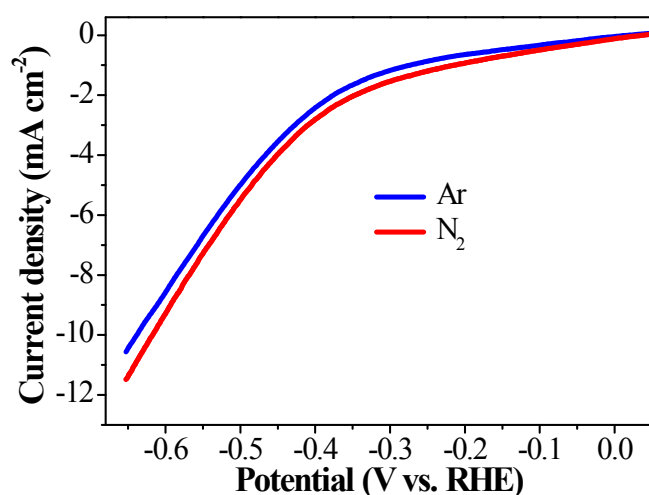
Fig. S6 LSV curves of Cu/AC catalyst in Ar- or N_2-saturated 0.1 M Na_2SO_4.
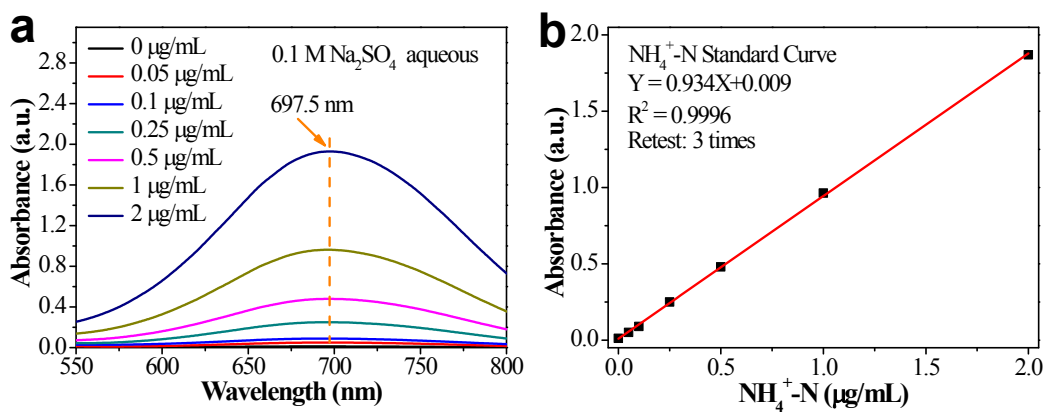
Fig. S7 (a) UV-Vis absorption spectra of various NH_4^+-N concentrations (0, 0.05, 0.1, 0.25, 0.5, 1, 2 and 4 μg mL^{-1}) after incubated for 1 h at room temperature. (b) The calibration curve used for calculation of NH_4^+-N concentration.
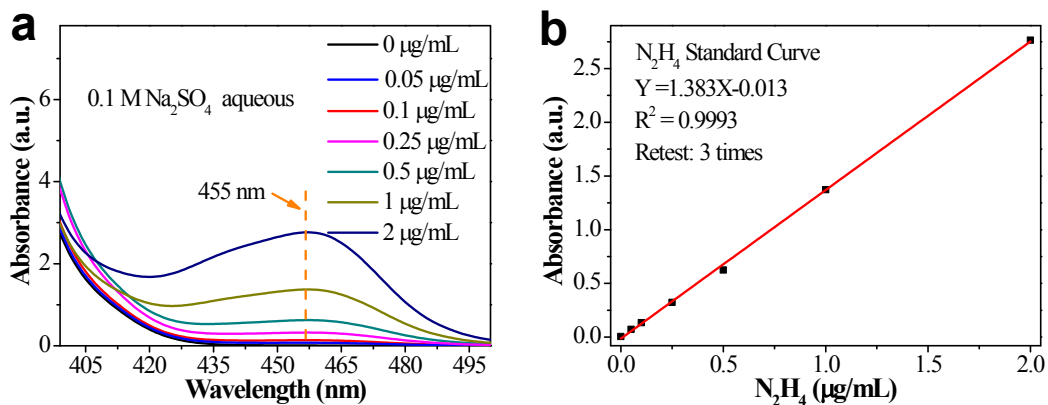
Fig. S8 (a) UV-Vis absorption spectra of various $N_2H_4 \cdot H_2O$ concentrations (0, 0.05, 0.1, 0.25, 0.5, 0.75, 1 and 2 μg mL^{-1}) after incubated for 20 min at room temperature. (b) The calibration curve used for calculation of $N_2H_4 \cdot H_2O$ concentrations.
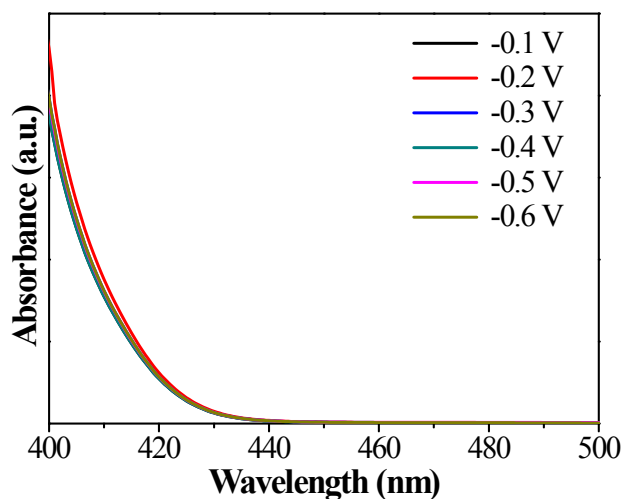
Fig. S9 UV-Vis absorption spectra of the samples after NRR measurement at different potentials in 0.1 M Na_2SO_4 electrolyte for 2 h.
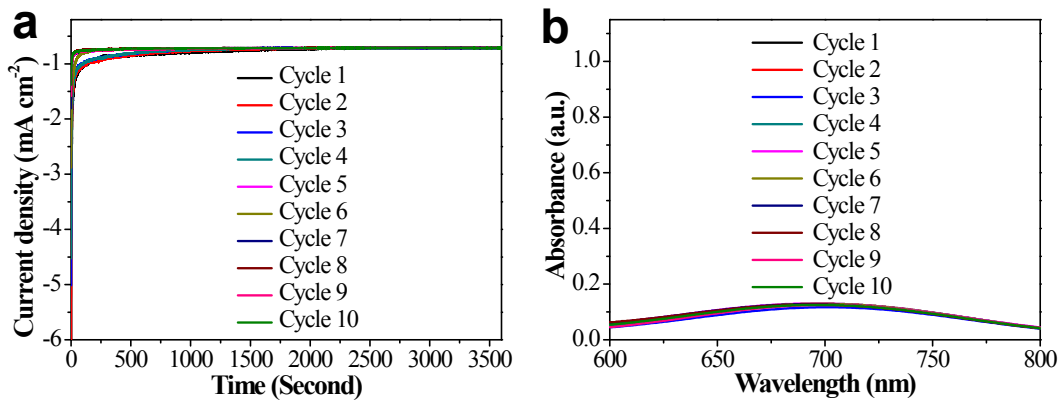
Fig. S10 (a) Time-dependent current density curves and (b) UV-Vis absorption spectra of the different cycle numbers of Cu/AC-S in 0.1 M Na_2SO_4 electrolyte for 1 h.
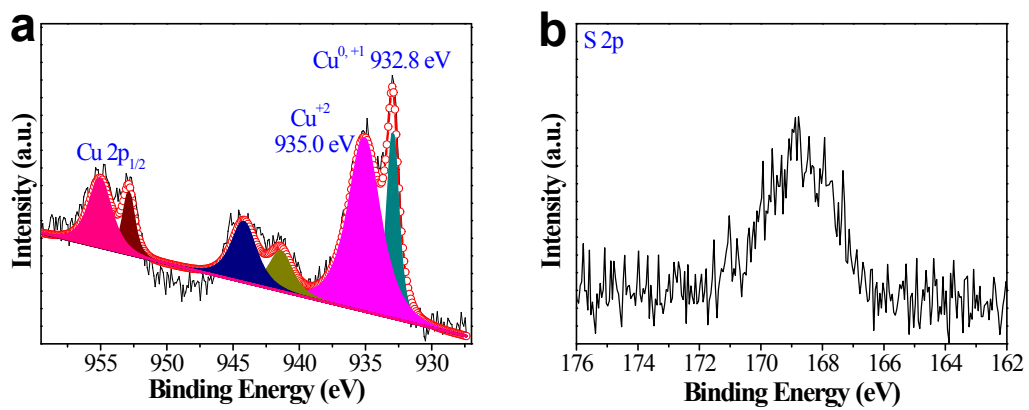
Fig. S11 (a) Cu 2p and (b) S 2p XPS spectra of Cu/AC-S after NRR.
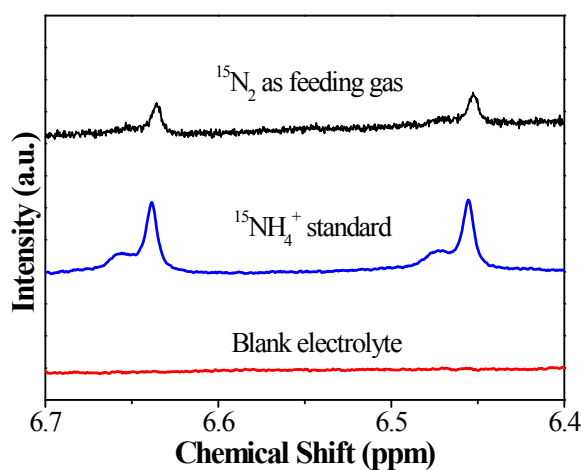
Fig. S12 NMR spectra of ^1H for the electrolytes after NRR test by using $^{15}N_2$ as feeding gas.
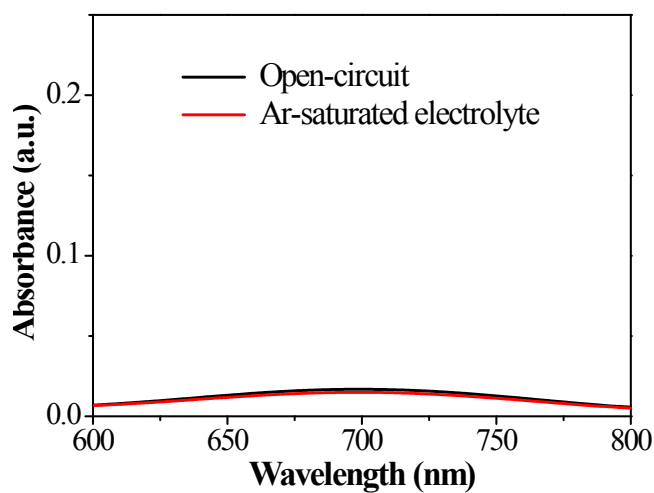
Fig. S13 UV-Vis absorption spectra of N_2-saturated 0.1 M Na_2SO_4 solution with the electrocatalyst for 2 h at open-circuit condition (open-circuit), and Ar-saturated 0.1 M Na_2SO_4 solution with the electrocatalyst at –0.3 V (*vs.* RHE) for 2 h (Ar-saturated electrolyte). All solutions were incubated with NH_3 color agent for 1 h before measurement.
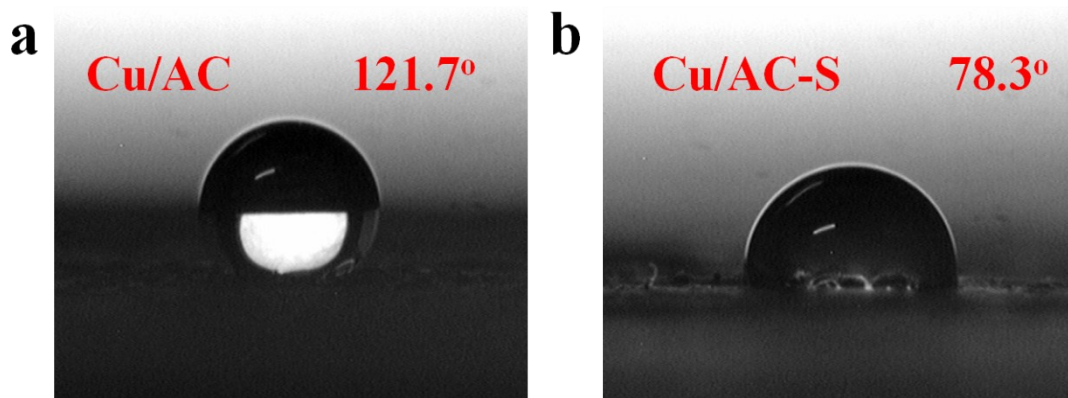
Fig. S14 Static contact angle measurements of (a) Cu/AC, (b) Cu/AC-S.
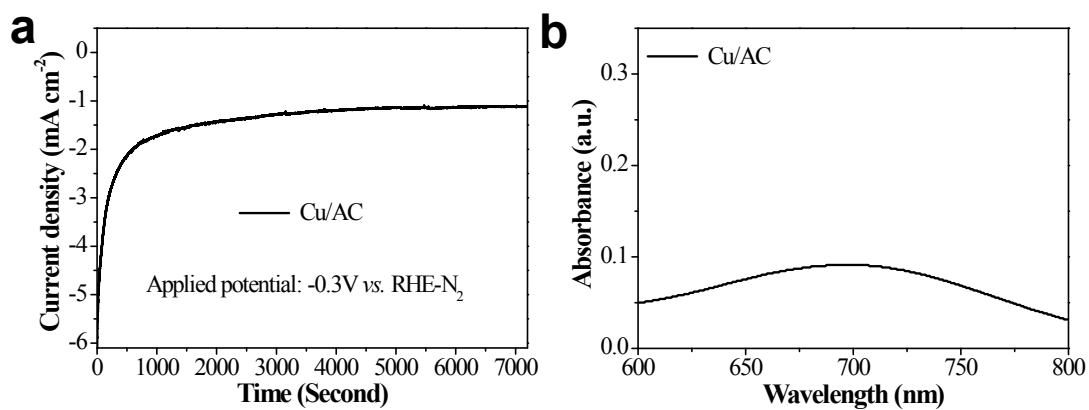
Fig. S15 (a) Time-dependent current density curve and (b) UV-Vis absorption spectra of of Cu/AC at −0.3 V (*vs.* RHE) for 2 h (N$_2$-saturated electrolyte).
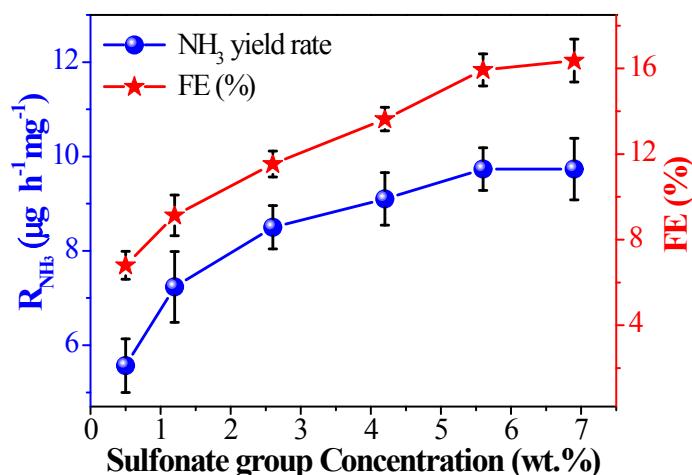
Fig. S16 NH$_3$ yield rate and corresponding FE for Cu/AC-S with different sulfonate group concentration (wt.%) at -0.3 V *vs.* RHE after 2 h electrolysis under ambient conditions.

References

1   J. Wang, L. Yu, L. Hu, G. Chen, H. Xin and X. Feng, *Nat. Commun.*, 2018, **9**, 1795.

2   D. Bao, Q. Zhang, F.-L. Meng, H.-X. Zhong, M.-M. Shi, Y. Zhang, J.-M. Yan, Q. Jiang and X.-B. Zhang, *Adv. Mater.*, 2017, **29**, 1604799.

3   M.-M. Shi, D. Bao, B.-R. Wulan, Y.-H. Li, Y.-F. Zhang, J.-M. Yan and Q. Jiang, *Adv. Mater.*, 2017, **29**, 1606550.

4   S.-J. Li, D. Bao, M.-M. Shi, B.-R. Wulan, J.-M. Yan and Q. Jiang, *Adv. Mater.*, 2017, **29**, 1700001.

5   M.-M. Shi, D. Bao, S.-J. Li, B.-R. Wulan, J.-M. Yan and Q. Jiang, *Adv. Energy Mater.*, 2018, **8**, 1800124.

6   H. Huang, L. Xia, X. Shi, A. M. Asiri and X. Sun, *Chem. Commun.*, 2018, **54**, 11427.

7   H.-M. Liu, S.-H. Han, Y. Zhao, Y.-Y. Zhu, X.-L. Tian, J.-H. Zeng, J.-X. Jiang, B. Y. Xia and Y. Chen, *J. Mater. Chem. A*, 2018, **6**, 3211.

8   M. Nazemi and M. A. El-Sayed, *J. Phys. Chem. Lett.*, 2018, **9**, 5160.

9   B. H. R. Suryanto, D. Wang, L. M. Azofra, M. Harb, L. Cavallo, R. Jalili, D. R. G. Mitchell, M. Chatti and D. R. MacFarlane, *ACS Energy Lett.*, 2019, **4**, 430.

10   H. K. Lee, C. S. L. Koh, Y. H. Lee, C. Liu, I. Y. Phang, X. Han, C.-K. Tsung and X. Y. Ling, *Sci. Adv.*, 2018, **4**, eaar3208.

11   H. Wang, H. Yu, Z. Wang, Y. Li, Y. Xu, X. Li, H. Xue and L. Wang, *Small*, 2019, **15**, 1804769.

12   Q. Qin, T. Heil, M. Antonietti and M. Oschatz, *Small Methods*, 2018, **2**, 1800202.

13   Y.-C. Hao, Y. Guo, L.-W. Chen, M. Shu, X.-Y. Wang, T.-A. Bu, W.-Y. Gao, N. Zhang, X. Su, X. Feng, J.-W. Zhou, B. Wang, C.-W. Hu, A.-X. Yin, R. Si, Y.-W. Zhang and C.-H. Yan, *Nat. Catal.*, 2019, **2**, 448.

14   Y. Liu, Y. Su, X. Quan, X. Fan, S. Chen, H. Yu, H. Zhao, Y. Zhang and J. Zhao, *ACS Catal.*,

2018, **8**, 1186.

15   C. Lv, Y. Qian, C. Yan, Y. Ding, Y. Liu, G. Chen and G. Yu, *Angew. Chem., Int. Ed.*, 2018, **57**, 10246.

16   C. Zhao, S. Zhang, M. Han, X. Zhang, Y. Liu, W. Li, C. Chen, G. Wang, H. Zhang and H. Zhao, *ACS Energy Lett.*, 2019, **4**, 377.

17   W. Qiu, X.-Y. Xie, J. Qiu, W.-H. Fang, R. Liang, X. Ren, X. Ji, G. Cui, A. M. Asiri, G. Cui, B. Tang and X. Sun, *Nat. Commun.*, 2018, **9**, 3485.

18   S. Chen, S. Perathoner, C. Ampelli, C. Mebrahtu, D. Su and G. Centi, *Angew. Chem., Int. Ed.*, 2017, **56**, 2699.

19   L. Zhang, X. Ji, X. Ren, Y. Ma, X. Shi, Z. Tian, A. M. Asiri, L. Chen, B. Tang and X. Sun, *Adv. Mater.*, 2018, **30**, 1800191.

20   D. Yang, T. Chen and Z. Wang, *J. Mater. Chem. A*, 2017, **5**, 18967.

21   Y. Liu, M. Han, Q. Xiong, S. Zhang, C. Zhao, W. Gong, G. Wang, H. Zhang and H. Zhao, *Adv. Energy Mater.*, 2019, **9**, 1803935.

22   P. Chen, N. Zhang, S. Wang, T. Zhou, Y. Tong, C. Ao, W. Yan, L. Zhang, W. Chu, C. Wu and Y. Xie, *Proc. Natl. Acad. Sci. USA*, 2019, **116**, 6635.

23   F. Wang, Y.-p. Liu, H. Zhang and K. Chu, *ChemCatChem*, 2019, **11**, 1441.

24   Y. Guo, Z. Yao, B. J. J. Timmer, X. Sheng, L. Fan, Y. Li, F. Zhang and L. Sun, *Nano Energy*, 2019, **62**, 282.

25   H. Jin, L. Li, X. Liu, C. Tang, W. Xu, S. Chen, L. Song, Y. Zheng and S.-Z. Qiao, *Adv. Mater.*, 2019, **0**, 1902709.

26   X. Wang, W. Wang, M. Qiao, G. Wu, W. Chen, T. Yuan, Q. Xu, M. Chen, Y. Zhang, X. Wang, J. Wang, J. Ge, X. Hong, Y. Li, Y. Wu and Y. Li, *Sci Bull*, 2018, **63**, 1246.

27   Z. Geng, Y. Liu, X. Kong, P. Li, K. Li, Z. Liu, J. Du, M. Shu, R. Si and J. Zeng, *Adv. Mater.*, 2018, **30**, 1803498.

28   H. Tao, C. Choi, L.-X. Ding, Z. Jiang, Z. Han, M. Jia, Q. Fan, Y. Gao, H. Wang, A. W. Robertson, S. Hong, Y. Jung, S. Liu and Z. Sun, *Chem*, 2019, **5**, 204.

29   L. Han, X. Liu, J. Chen, R. Lin, H. Liu, F. Lü, S. Bak, Z. Liang, S. Zhao, E. Stavitski, J. Luo, R. R. Adzic and H. L. Xin, *Angew. Chem., Int. Ed.*, 2019, **58**, 2321.

30   M. Wang, S. Liu, T. Qian, J. Liu, J. Zhou, H. Ji, J. Xiong, J. Zhong and C. Yan, *Nat. Commun.*, 2019, **10**, 341.

31   F. Lü, S. Zhao, R. Guo, J. He, X. Peng, H. Bao, J. Fu, L. Han, G. Qi, J. Luo, X. Tang and X. Liu, *Nano Energy*, 2019, **61**, 420.

32   L. Hui, Y. Xue, H. Yu, Y. Liu, Y. Fang, C. Xing, B. Huang and Y. Li, *J. Am. Chem. Soc.*, 2019.